



Mathematical modelling of stress-strain state of steel-concrete beams with combined reinforcement

Jacek Selejdak^{1*}, Taras Bobalo², Yaroslav Blikharsky³, Iryna Dankevych²

¹ Czestochowa University of Technology, Faculty of Civil Engineering, 69 st. Dabrowskiego, 42-201 Czestochowa, Poland; jacek.selejdak@pcz.pl

² Lviv Polytechnic National University, Department of Building Constructions and Bridges, 12 st. S. Bandera, Lviv, 79013, Ukraine; taras.v.bobalo@lpnu.ua (TB); iryna.p.dankevych@lpnu.ua (ID)

³ Lviv Polytechnic National University, Department of Highways and Bridges, 12 st. S. Bandera, Lviv, 79013, Ukraine; yaroslav.z.blikharsky@lpnu.ua

*Correspondence: jacek.selejdak@pcz.pl

Article history

Received 14.10.2022

Accepted 04.01.2023

Available online 20.02.2023

Keywords

combined reinforcement
high-strength rebar
steel-concrete structures
design of RC structures
external reinforcement

Abstract

Most of the modern computer software for the building structures` calculation is based on mathematical dependencies which make it possible to analyse rather complex stress-strain state of structures subjected to loading. As a rule, the calculation is based on the finite element method and is reduced to the calculation of deformations arising in structures due to the action of external forces with the use of real strain diagrams of materials, σ - ε diagrams for concrete and reinforcement. Modern normative regulations for reinforced concrete structures` calculation are also based on the deformation model using material deformation diagrams, which are as close to the real ones, as possible. Therefore, this study was aimed to investigate in more detail the stress-strain state and the physical essence of the processes occurring in reinforced concrete structures with combined reinforcement according to mathematical approaches and regulations of DBN B.2.6-98:2009 and DSTU B. In 2.6-156:2010. Namely, in the research is analysed the combined reinforcement of S245 steel tapes and A1000 rebar, which is used in the production of reinforced concrete elements. The results of mathematical modelling were compared with the calculation results, according to DBN B.2.6-98: 2009 and DSTU B. B 2.6-156:2010, as well as with field experimental data. Therefore, the conclusion could be made, whether it is possible to use this technique with sufficient accuracy to calculate reinforced concrete structures with combined reinforcement.

DOI: 10.30657/pea.2023.29.13

1. Introduction

Reinforced concrete structures, subjected to bending, have occupied the prevailing position in construction practice (Blikharsky et al., 2021). The reinforced concrete should be considered as the artificial material, which properties could be predefined based on consideration of particular application conditions, which requires detailed analytical investigation (Blikharsky et al., 2021). In the works (Vavruš et al., 2019) research was conducted, aiming to indicate the need for control load testing of bridge structures to assess the accuracy of calculations and mathematical modeling in the design of structures. An important factor that will affect the accuracy of the mathematical model is the presence of damage and defects (Lobodanov et al., 2019), the impact of which cannot be taken

into account without experimental data. According to research of (Blikharsky et al., 2021), an important problem for operated reinforced concrete structures is intensive environmental impact, which could be the reason for local destruction and failure of structures. The paper (Vegeera et al., 2021) describes an improved method of calculating reinforced concrete beams, with damages in the stretched reinforcement that occurred during loading. Also, the work (Blikharsky et al., 2021) should be noted, where changes of rebar stress-strain state due to corrosion fatigue damages.

Studies devoted to determination of the load-bearing and carrying of prefabricated bridge bended structures were conducted for real bridges in Slovakia (Koteš et al., 2021). The calculation was performed according to Eurocode standards,



© 2023 Author(s). This is an open access article licensed under the Creative Commons Attribution (CC BY) License (<https://creativecommons.org/licenses/by/4.0/>).

which take into account the modified reliability levels and partial safety factors. According to the results of analytical calculation with the use of probabilistic approach, the decrease in the reliability and durability of the bridge was identified. Also, the relationship between the fatigue crack size and change of the resistance and the reliability of the cross section over time was identified (Koteš and Vičan, 2021).

One of the factors in the modeling of bridge structures is the need to take into account changes in the physical and mechanical characteristics of materials (Song et al., 2022). The analysis of the influence of various factors on the process of chloride penetration into the concrete structure was performed. Also, the difficulty of introduced mathematical models may be caused by the use of new or modified materials for the structure manufacturing (Federowicz et al., 2021; Mao et al., 2019). The article (Czajkowska et al., 2020) analyzes the influence of different humidity conditions on selected strength properties of hardened steel-fiber concrete (such as Young's modulus and compressive strength of concrete). The analysis shows that the value of the Young's modulus of concrete that hardens at 100% humidity is the highest. In all these cases for mathematical modeling it is necessary to specify experimentally determined characteristics of materials, determined with the required reliability.

An engineering method for calculating the bearing capacity of the supporting sections of solid monolithic reinforced concrete tape beams, which unite pressed or driven reinforced concrete piles into single foundation structure (Kos et al., 2022). The authors evaluated the influence of structural factors in long-span studied elements, and with the use of computer software "Lira-Sapr" modeled their work under loading. Study was aimed to clarify the stress-strain state and confirm the scheme of their destruction adopted in the physical model.

Development and testing of mathematical models of reinforced concrete beams' cracking using the software "COMPEX" were carried out to determine the width of normal cracks and the length of the projection of dangerous inclined cracks (Karpiuk et al., 2021). The models are based on experimental studies of T-shaped prestressed beam structures. Based on the obtained data, an empirical expression is proposed to determine the projection of a dangerous inclined crack for such beams.

This paper also discusses the impact of an eccentric crack. The numerical approach was based on the combination of general finite element and a multiparameter form of the maximum tangential stress criterion. This generalized method is especially suitable for materials with specific (elastoplastic, quasi-brittle, etc.) fracture behavior. As the result of the research, some recommendations for the use of one-parameter / multiparameter fracture mechanics were given (Malíková et al., 2020).

An important issue is the implementation of mathematical modeling of structures reinforced with composite materials (Inytskyi et al., 2020). The use of composite reinforcement has the number of advantages over classic steel reinforcement. For instance, coefficients of thermal expansion of reinforcement and concrete are quite close, which prevents the formation of cracks when the temperature changes.

The complex stress-strain state of inclined sections, in the case of their strengthening, is the difficult case of theoretical calculation and mathematical modeling (Blikharsky et al., 2018). Experimental studies of reinforced concrete beams show deviations from the calculation models, which requires clarification.

The different stress-strain state of the main structure and the reinforcement system complicates the mathematical modeling, because such a stress-strain state will be different from the real one (Borysiuk and Ziatiuk, 2020). The special case is the modeling of the stress-strain state of structures, in the case of their strengthening, when the characteristics of the strengthening material differs significantly (Azizov et al., 2019). In this case, correct mathematical modeling requires determination of the parameters of the compatible stress-strain state and the joint operation of such a composite structure. The paper (Azizov et al., 2020) describes the method of calculating of masonry structures that are strengthened with reinforced concrete slabs. Studies show that in the case of high-stiffness joints, the structure can be calculated as monolithic, taking into account the characteristics of two different materials. In the general case when constructions need to be calculated as separate, it is necessary to add the characteristics of the joint or adhesive layer to the mathematical model (Blikharsky, 2019).

Experimental studies of masonry structures, strengthened with steel sheets, in the form of indirect reinforcement showed that with the same area of indirect reinforcement by steel bars or sheets, the strength of elements with sheets-strengthening is on average 40% higher (Pavlikov, et al., 2020). Such results should be taken into account when conducting mathematical modeling, calculation or design of such structures.

The study of the influence of dynamic loading on structures of various kinds is a common practice in mathematical modeling (Panchenko et al., 2021). This case of loading is difficult for experimental testing or manual calculation, because the dynamic load varies according to the certain law and accurate research could be performed only by modeling the stress-strain state of such structures.

The factors, mentioned above, lead to changes in the reliability of structures. Modeling of real operating conditions of structures is given in (Khmil et al., 2020). Therefore, the number of controlled random parameters were included in the theory of calculations, namely: strength of materials, geometric cross-sectional parameters, as well as the level of load in the case of structural strengthening. The presence of the load level simulates the real operating conditions of the structure during its strengthening (Khmil et al., 2021).

The above cases show the importance of the study of structures through experimental tests and their subsequent mathematical modeling, to create adequate models and further use the digital data.

2. Problem formulation

When modeling structures of any complexity, three types of finite elements are usually used:

- linear element (Fig. 1a), which in this study is identified with the steel bar, perceives only axial tension or compression and has four degrees of freedom;
- plane quadrangular or triangular element, which in this study is identified with concrete and is in a plane stress state and has eight degrees of freedom (Fig. 1b);
- three-dimensional element, also very often identified with concrete structures, but in this study, such elements were abandoned.

The individual elements are joined by nodes. Each node has two possible displacement directions - u and v . The linear i -th finite element is described by the coordinates of two points (i, j), has the linear length - l_i , cross-sectional area - A_i and the initial modulus of elasticity - E_{soi} . It is generally assumed, that the linear element is subjected only to tensile and compressive deformations, and does not perceive bending deformations.

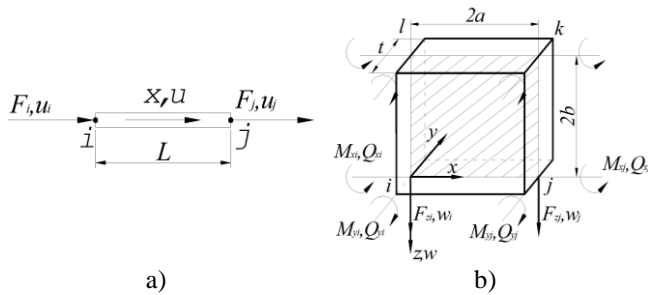


Fig. 1. Finite elements: a – linear; b – plane

The plane i -th finite element is characterized by coordinates of four nodes (i, j, k, l), area - A_i , thickness - t_{pl} , modulus of elasticity - E_x, E_y, E_1, E_2 (E_1, E_2 values are required for calculation of shear modulus G).

Differential expressions for dependence between deformations and displacements are given by the equations of the theory of elasticity, also known as Cauchy equation.

$$\varepsilon_x = \frac{\partial u}{\partial x} ; \quad \varepsilon_y = \frac{\partial v}{\partial y} \quad (1)$$

The plane problem of the theory of elasticity considers two partial cases of the stress-strain state - the plane deformation and the plane stress state. In both cases, all the parameters of the stress-strain state depend on only two coordinates, because the considered area is two-dimensional.

For the plane problem of the theory of elasticity, the vectors of displacement and external load are two-dimensional, and the vectors of stresses and strains contain three components:

$$\bar{u} = \begin{Bmatrix} u \\ v \end{Bmatrix} ; \quad \bar{\sigma} = \begin{Bmatrix} \sigma_x \\ \sigma_y \\ \tau_{xy} \end{Bmatrix} ; \quad \bar{\varepsilon} = \begin{Bmatrix} \varepsilon_x \\ \varepsilon_y \\ \gamma_{xy} \end{Bmatrix} \quad (2)$$

For isotropic material the basic relations of the plane stress state could be given in the following form:

Matrix of dependence of deformations and displacements:

$$\bar{\varepsilon} = [B] \cdot \bar{u} \quad (3)$$

The matrix operator of Cauchy differential equations [B] will look like:

$$[B] = \begin{Bmatrix} \varepsilon_x \\ \varepsilon_y \\ \gamma_{xy} \end{Bmatrix} = \begin{bmatrix} \frac{\partial}{\partial x} & 0 \\ 0 & \frac{\partial}{\partial y} \\ \frac{\partial}{\partial y} & \frac{\partial}{\partial x} \end{bmatrix} \cdot \begin{Bmatrix} u \\ v \end{Bmatrix}; \quad (4)$$

Matrix of dependence of stresses and deformations:

$$\bar{\sigma} = [D] \cdot \bar{\varepsilon}; \quad (5)$$

The matrix operator of the transition from strain to stress [D] will have the form:

$$[D] = \begin{Bmatrix} \sigma_x \\ \sigma_y \\ \tau_{xy} \end{Bmatrix} = \frac{E}{1-\mu^2} \cdot \begin{bmatrix} 1 & \mu & 0 \\ \mu & 1 & 0 \\ 0 & 0 & \frac{1-\mu}{2} \end{bmatrix} \cdot \begin{Bmatrix} \varepsilon_x \\ \varepsilon_y \\ \gamma_{xy} \end{Bmatrix}, \quad (6)$$

where [B] – material stiffness matrix; [D]- matrix of elastic characteristics.

Deformations ε_x and ε_y in the case of plane stress state will have the following form:

$$\begin{cases} \varepsilon_x = \frac{\sigma_x}{E_x} - \mu \frac{\sigma_y}{E_y} \\ \varepsilon_y = \frac{\sigma_y}{E_y} - \mu \frac{\sigma_x}{E_x} \end{cases} \text{ therefore } \begin{cases} \sigma_x = \frac{E_x}{1-\mu^2} (\varepsilon_x + \mu \varepsilon_y) \\ \sigma_y = \frac{E_y}{1-\mu^2} (\varepsilon_y + \mu \varepsilon_x) \end{cases}, \quad (7)$$

Secant deformation modulus E_x, E_y, E_1, E_2 and shear modulus G for i -th quadrilateral finite element could be determined from the equations:

$$E_x = \frac{f\left(\frac{\varepsilon_x + \mu \varepsilon_y}{1-\mu^2}\right)}{\frac{\varepsilon_x + \mu \varepsilon_y}{1-\mu^2}}, \quad E_y = \frac{f\left(\frac{\varepsilon_y + \mu \varepsilon_x}{1-\mu^2}\right)}{\frac{\varepsilon_y + \mu \varepsilon_x}{1-\mu^2}}, \quad E_1 = \left| \frac{f(\gamma)}{\gamma} \right|, \quad (8)$$

$$E_2 = \left| \frac{f(-\gamma)}{-\gamma} \right| \quad (9)$$

$$G = \frac{E_1 E_2}{(1+\mu)(E_1 + E_2)} \quad (9)$$

where: $\frac{\varepsilon_x + \mu \varepsilon_y}{1-\mu^2}, \frac{\varepsilon_y + \mu \varepsilon_x}{1-\mu^2}$ – relative deformations in a quadrangular finite element;

$f(\varepsilon_x)$ and $f(\varepsilon_y)$ – stresses σ_x and σ_y , obtained from the real deformation diagram for i -th quadrangular finite element;

$f(\gamma)$ and $f(-\gamma)$ – normal stresses, which correspond to deformations;

l, h – width and height of quadrangular finite element;

t, z – constant values, which are assumed to be equal respectively $0.5t$ and $0.5z$ for the coordinate of the finite element center;

$\mu=0.3$ – Poisson's ratio;

$\gamma = (1-t) \cdot (U_i - U_j)/l + t \cdot (U_k - U_j)/l + (1-z) \cdot (V_j - V_i)/h + z \cdot (V_k - V_i)/h$ – shear angle;

$V_i, U_i, V_j, U_j, V_k, U_k, V_l, U_l$ – displacement of nodes i, j, k, l .

The calculation model for the analysis of the work of reinforced concrete beams with combined reinforcement has the form of set of linear and rectangular plane finite elements, the total area of which corresponds to the size of the experimental beams. The linear finite elements perform the function of steel bars, which are the reinforcement of the beam in the lower and upper zones. The rectangular plane finite element is assigned the characteristics of concrete.

3. Description for real σ - ε diagrams for reinforcement

The accuracy of the reinforced concrete structures` calculation depends on the accuracy of the input information about the materials` physical and mechanical characteristics. Therefore, real " σ - ε " diagrams of the materials` stress-strain state were used to perform the calculations.

For a more accurate description of the deformation diagram of high-strength and usual reinforcement, it was conditionally divided into four sections (Fig. 2).

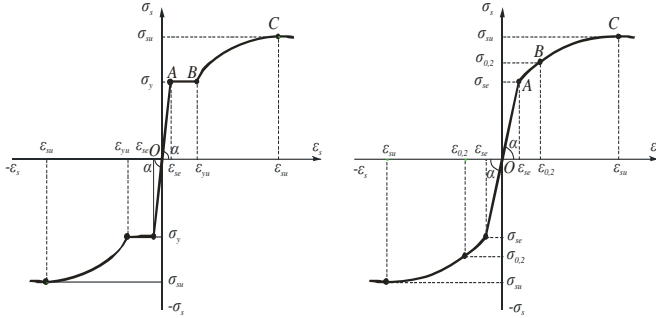


Fig. 2. Mathematical representation of real deformation diagrams of reinforcement with physical yield strength (a) and reinforcement with conditional yield strength (b)

The first region OA of both diagrams corresponds to the elastic work of steel with the initial modulus E_0 , and is limited by the yield strength of mild steel or conditional yield strength for high-strength reinforcement, which is equal to $\sigma_{se} \leq 0.7\sigma_{0.2}$. In these regions Hooke's law is valid and linear dependence $\sigma_k = \varepsilon_k E_k$ could be applied.

$$0 \leq \varepsilon_k < \frac{0.7\sigma_{0.2}}{E_k}, \quad (10)$$

For mild reinforcement with physical yield region the linear dependence $\sigma_i = \varepsilon_i E_i$ could be accepted within following limits:

$$0 \leq \varepsilon_i < \frac{0.6\sigma_y}{E_i}. \quad (11)$$

The second section is curvilinear, from the beginning of the elastic limit to the beginning of the yield strength, and could be described with the use of the quadratic EKB-FIP dependence:

$$\sigma_s = \frac{f_{ud}(k\eta - \eta^2)}{1 + (k-2)\eta}, \quad (12)$$

where $\eta = \frac{\varepsilon_{si}}{\varepsilon_{su}}$ - the value, which indicates the intensity of strain increase for i-th region; ε_{si} , ε_{su} - the strain value, corresponding to the maximum compression stress; k - coefficient of elastic-plasticity, indicating the point at which the curve reaches the elastic limit:

$$k = \frac{E_k^2 \sigma_y^2 - 1.2\sigma_y E_k \varepsilon_y + 0.7\sigma_{0.2}^2}{0.4\sigma_y E \varepsilon_y}, \quad (13)$$

$$k = \frac{E_i^2 \sigma_y^2 - 1.2\sigma_y E_i \varepsilon_y + 0.6\sigma_y^2}{0.4\sigma_y E \varepsilon_y}. \quad (14)$$

The third region corresponds to the yield region. It could be described by line, parallel to X-axis.

For high-strength reinforcement with conditional yield strength:

$$\sigma_i = \sigma_{un}, \varepsilon_{0.2} \leq \varepsilon_i < \varepsilon_{un}, \quad (15)$$

For mild reinforcement with physical yield region:

$$\sigma_i = \sigma_y, \varepsilon_y \leq \varepsilon_i < \varepsilon_{yn}. \quad (16)$$

The fourth section runs from the end of the yield strength until the tensile strength. The beginning of the curve corresponds to the beginning of the coordinates, the intermediate point is the end of the yield region, and the top of the curve is the temporary limit strength.

Coefficient k could be obtained from the condition of passing the curve through the specified points:

$$k = \frac{\sigma_y^2 - \eta_0^2 - 2\eta_0}{\eta_0 - \sigma_y \eta_0}, \text{ where } \eta_{ui} = \frac{\varepsilon_{yn}}{\varepsilon_u}. \quad (17)$$

4. Description of real σ - ε diagrams for concrete

The main physical characteristics of linear and quadrangular finite elements are the initial modulus of elasticity of finite elements, the fixing scheme in the nodes, the control points of relative deformations and stresses according to the obtained real diagrams.

In order to describe the process of deformation σ - ε of concrete, the quadratic dependence according to the proposals of DBN B.2.6-98: 2009 was used. The analysis of the obtained results of curves` approximation showed their similarity with the accuracy within 1.2-3.2% with the values of real diagrams obtained from testing prisms.

For the region of concrete, subjected to compression (Fig. 3) the equation has the following form, according to DBN B.2.6-98: 2009:

$$\sigma_{bi} = \frac{f_{ck,prism}(k_0\eta - \eta^2)}{1 + (k_0 - 2)\eta}, \quad (18)$$

where $\eta = \frac{\varepsilon_{bi}}{\varepsilon_{bu}}$ - the value, which indicates the intensity of strain increase for i-th region of concrete; ε_{bi} - the strain value, corresponding to the maximum compression stress; k_0 - coefficient, which takes into account plastic strain in concrete, $f_{ck,prism}$ - prism strength of concrete on the 28th day after manufacturing.

To build the ascending graph, an additional point was introduced, which corresponded to the initial modulus of deformation of concrete E_{b0} . It was for stresses about $\sigma_b = 0.3R_b$. Therefore, the stress-strain equations had the following form:

$$\varepsilon_b = \frac{\sigma}{E_{ck}} = \frac{0.3 \cdot f_{ck,prism}}{E_{ck}}, \quad (19)$$

therefore

$$\eta_0 = \frac{0.3 \cdot f_{ck,prism}}{\varepsilon_{bu} E_{ck}}, \quad (20)$$

Therefore, the elastic-plasticity coefficient of ascending graph for concrete k is equal to:

$$k = \frac{\eta_0^2 - 0.6\eta_0 + 0.3}{0.7\eta_0}. \quad (21)$$

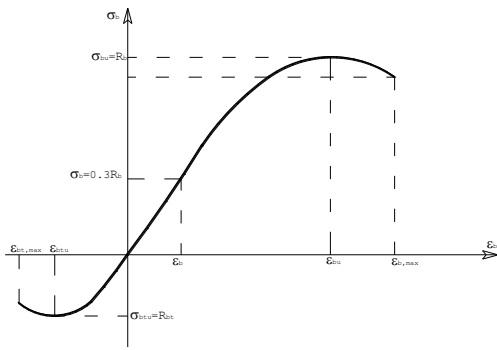


Fig. 3. Mathematical interpretation of the real deformation diagrams for concrete

In order to identify the maximum point of ascending graph for concrete the following equation was introduced, which according to [Błąd! Nie można odnaleźć źródła odwołania.] is in good agreement with experimental data:

$$\epsilon_{bu} = \left(3.6f_{ck,prism} - 3 \left[\frac{f_{ck,prism}}{36} \right]^5 + 51 \right) 10^{-5}, \quad (22)$$

where the starting point of the ascending branch was assumed at the coordinate origin.

In order to describe the descending branch, an additional control point was introduced, which corresponded to the final value of concrete deformations, taking into account, that the concrete strain $\epsilon_{b,max}$ was introduced by equation:

$$\epsilon_{b,max} = \frac{f_{ck,prism}}{(10+2.7f_{ck,prism})}^{-2}, \quad (23)$$

Therefore, the elastic-plasticity coefficient of ascending graph for concrete k if $\epsilon_{b,max}$ corresponds to stress $\sigma_b = 0.8f_{ck,prism}$ is equal to:

$$k_1 = \frac{\eta_{01}^2 - 1.6\eta_{01} + 0.8}{0.2\eta_{01}}. \quad (24)$$

for stretched region of the concrete diagram he dependence could be used, which has the form, similar to the compression:

$$\sigma_{bi} = \frac{f_{ctk,0.05}(k_0\eta - \eta^2)}{1 + (k_0 - 2)\eta}, \quad (25)$$

where coefficient η was taken from the condition $\eta = \frac{\epsilon_{ck}}{\epsilon_{btu}}$, where ϵ_{ck} - the tension strain of concrete, which correspond to the maximum tension stress $f_{ctk,0.05}$.

4. Experimental investigation

In order to verify the developed mathematical model, 8 reinforced concrete beams with an estimated span of 2400 mm, cross section 120x240 mm and 2600 mm length were designed, manufactured and tested. Beams were designed according to single span scheme, with two supports loaded with two concentrated forces in thirds of their span (Fig. 4).

At the first stage, it was aimed to design beams with different percentages of cross-section reinforcement and with different ratio in the amount of high-strength rebar and tape reinforcement, however the condition was fulfilled, that their

strength according to the DSTU BV.2.6-156: 2010 calculation should be the same, that is, the destructive load for them was assumed to be the same. This was done for the convenience of comparing the experimental results and obtaining more accurate results.

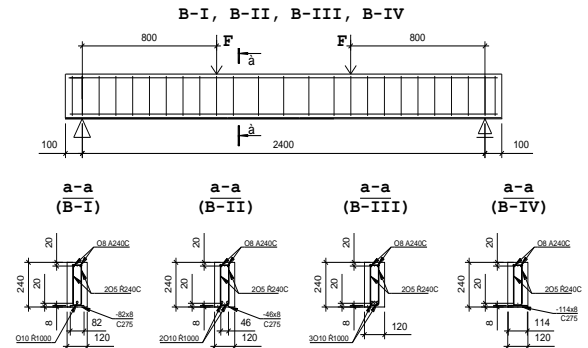


Fig. 4. Reinforcement frames of experimental beams

In the stretched zone of experimental samples the combined reinforcement was used, containing smooth S275 steel tapes of 8 mm width and high-strength A1000 rebar of periodic profile with \varnothing 10 mm. The reinforcement of the compressed zone of experimental samples was designed from periodic profile rebar of \varnothing 8 mm and A400S class. Transverse reinforcement, which was also the anchors for smooth tape S275 reinforcement were steel bars of 5 mm diameter and A240S class, with 70 mm - spacing at the supports and 100 mm-spacing in the area of pure bending. Design concrete grade was C35/45.

The designed beams were divided into four series, in order to increase the reliability of the test results, each series consisted of two identical beams, which were manufactured and tested under the same conditions (Table 1).

Table 1. Characteristics of the test samples

Marking of the beams	B-I-1, B-I-2	B-II-1, B-II-2	B-III-1, B-III-2	B-IV-1, B-IV-2
Cross-section width b, mm	120	120	120	120
height h, mm	240	240	240	240
area A, cm ²	288	288	288	288
Reinforcement of stretched zone – longitudinal S275 steel tape				
width b _s , mm	82	46	-	114
thickness t _s , mm	8	8	-	8
area A _s , cm ²	6.56	3.68	-	9.12
Reinforcement of stretched zone – longitudinal steel bars				
Number and diameter of steel bars \varnothing_s , mm	1 \varnothing 10 A1000	2 \varnothing 10 A1000	3 \varnothing 10 A1000	-
area A _{sb} , cm ²	0.785	1.570	2.355	-
$R_s(f_{yk})A_{sb}$ of steel bar	31.2%	61.9%	100%	0%
$R_s(f_{yk})A_{st}$ of tape	68.8%	38.1%	0%	100%
total reinforcement ratio	2.77%	1.97%	0.89%	3.45%
Reinforcement of compressed zone – longitudinal steel bars				
Number and diameter of steel bars \varnothing_s , mm	2 \varnothing 8 A400S	2 \varnothing 8 A400S	2 \varnothing 8 A400S	2 \varnothing 8 A400S
area A _{s'} , cm ²	1.005	1.005	1.005	1.005
Transverse steel bars				
Number and diameter of steel bars \varnothing_{sw} , mm	2 \varnothing 5 A240S	2 \varnothing 5 A240S	2 \varnothing 5 A240S	2 \varnothing 5 A240S
area A _{sw} , cm ²	0.392	0.392	0.392	0.392
spacing S, mm	70	70	70	70

In the beams of series B-I and B-II the combined reinforcement of the stretched zone contained A1000S class steel bars and S275 steel tape. In the beams of series B-III and B-IV combined reinforcement was not used, they served as a kind of standard samples for further comparison and analysis of the results of their work with the results of beams B-I and B-II. As the working longitudinal reinforcement of the stretched zone in beams of series B – III only high-strength steel bars were used, namely, three steel bars of 10 mm diameter and A1000 class. In beams of series B – IV, was used only tape reinforcement of S275 class and 8 mm thickness.

4. Comparison of the experimental test results with the calculation of the mathematical model

Described above computer method of calculation allowed to obtain the mathematical apparatus for describing and determining the stresses` and strains` values of concrete and working reinforcement at all stages of loading the structure until its destruction.

Results of theoretical calculations and experimental study are given in Table 2 - 4.

Obtained theoretical results, according to mathematical model with sufficient accuracy correspond to experimental data, which confirms the possibility of its usage for calculation of steel-concrete structures with combined reinforcement.

As could be seen from the results, the proposed computer calculation with sufficient accuracy estimates the load-bearing capacity of reinforced concrete beams with combined reinforcement, the deviation from the experimental data does not exceed 5.9% (Table 2).

Table 2. Comparison of experimental, theoretical according to mathematical model and calculated normative values of experimental beams` bearing capacity

Beams marking	Experimental result M_{dr1} at yielding of tape reinforcement, kNm		Value of M_{EOM1} at yield point of tape reinforcement, kNm		Load-bearing capacity (yield point of high-strength reinforcement, destruction of the compressed zone of concrete)		Experimental value M_{dr2} when the bearing capacity is exhausted, kNm		According to DBN.V.2.6-98:2009 M_{DBN} , kNm		According to computer calculation $M_{EOM_{max}}$, kNm	
	M_{dr1}	$(M_{dr1}-M_{EOM1})/M_{dr1}$, %	M_{EOM1}	$(M_{dr1}-M_{EOM1})/M_{dr1}$, %	M_{dr2}	$(M_{dr2}-M_{DBN})/M_{dr2}$, %	M_{DBN}	$(M_{dr2}-M_{DBN})/M_{dr2}$, %	$M_{EOM_{max}}$	$(M_{dr2}-M_{EOM_{max}})/M_{dr2}$, %		
B-I-1	42.70	-1.9	43.5	43.5	51.52	0.3	51.38	51.38	51.4	0.2		
B-I-2	43.60	0.2	43.5	43.5	52.64	2.4	51.38	51.38	51.4	2.4		
B-II-1	31.10	3.2	30.1	30.1	55.20	5.6	52.10	52.10	52.3	5.3		
B-II-2	31.10	3.2	30.1	30.1	52.40	0.6	52.10	52.10	52.3	0.2		
B-III-1	-	-	-	-	55.36	4.5	52.85	52.85	53.7	3.0		
B-III-2	-	-	-	-	57.04	7.3	52.85	52.85	53.7	5.9		
B-IV-1	51.49	2.1	50.4	50.4	51.49	2.4	50.25	50.25	50.4	2.1		
B-IV-2	50.57	0.3	50.4	50.4	50.57	0.6	50.25	50.25	50.4	0.3		

The values of the bending moments, that cause the formation of normal cracks, obtained by the numerical model, also have good similarities with experimental data, the deviation does not exceed 5.0%. Detailed data is given in Table 3.

Computer computation in the Turbo Pascal 7.0 environment with the use of finite element method, taking into account the real “ σ - ϵ ” deformation diagrams of materials corresponds to the work of the real structure reinforced by the rebar with external tape reinforcement.

This proves that the calculation model allows to estimate with sufficient accuracy the strength and deformability of reinforced concrete structures with combined reinforcement.

When determining the deflections, the satisfactory coincidence of results was obtained at all stages of structural loading (Table 4). During field tests, based on the results of mathematical modeling, it was possible to predict the work of the structure, compare the increase in deflections, cracks and control the yielding point of the tape reinforcement, which had its impact on samples` performance.

Table 3. Comparison of experimental, theoretical according to mathematical model and calculated normative values of experimental beams` fracture moments

Beams marking	Fracture moments of experimental beams				
	Experimental $M_{d_{crc}}$, kN*m	According to DBN V.2.6-98:2009 M_{DBN} , mm	$(M_{d_{crc}}^{d_{crc}} - M_{DBN}^{d_{crc}})/M_{d_{crc}}^{d_{crc}}$, %	According to mathematical model $M_{d_{crc}}^{mod}$, kN*m	$(M_{d_{crc}}^{d_{crc}} - M_{d_{crc}}^{mod})/M_{d_{crc}}^{d_{crc}}$, %
B-I-1	6.9		14.2		2.0
B-I-2	7.15	5.92	17.2	7.04	-1.5
B-II-1	8.00	6.12	23.5	7.71	-3.6
B-II-2	7.46		18.0		3.4
B-III-1	11.67		18.1		-4.0
B-III-2	10.99	5.26	6.1	11.2	1.9
B-IV-1	39.16		11.9		-5.0
B-IV-2	39.00	7.12	10.1	37.2	-4.6

Table 4. Comparison of experimental, theoretical according to mathematical model and calculated normative values of experimental beams` bearing capacity

Beams marking	Experimental f^1 , mm	According to DBN V.2.6-98:2009, f^{DBN} , mm	$(f^{DBN} - f^1)/f^1$, %	According to mathematical model, f^{mod} , mm	$(f^{mod} - f^1)/f^1$, %
B-I-1	2.21	2.15	-2.7	2.1	-5.0
B-I-2	2.35	2.15	-8.5	2.1	-10.6
B-II-1	4.81	4.5	-6.4	4.1	-14.8
B-II-2	3.98	4.5	13.1	4.1	3.0
B-III-1	8.25	8.9	7.9	8.2	-0.6
B-III-2	9.64	8.9	-7.7	8.2	-14.9
B-IV-1	1.94	.12	9.3	2.1	8.2
B-IV-2	2.08	.12	1.9	2.1	1.0

Table 4. Comparison of experimental, theoretical according to mathematical model and calculated normative values of experimental beams' bearing capacity (continue)

Beams marking	Experimental f_{t1}^d , mm	According to DBN V.2.6-98:2009, F_{DBN1} , mm	$(f_{DBN1}^d - f_{t1}^d) / f_{t1}^d$, %	According to mathematical model, F_{mod1} , mm	$(f_{mod1}^d - f_{t1}^d) / f_{t1}^d$, %
		0.7 M _{dr2}			
B-I-1	4.55	5.5	20.9	5.2	14.3
B-I-2	5.08		8.3		2,4
B-II-1	9.44	10.4	10.2	9.8	3.8
B-II-2	9.56		8.8		2.5
B-III-1	20.32	21.8	7.3	22.1	8,8
B-III-2	21.57		1.1		2,5
B-IV-1	4.15	4.4	6.0	4.4	6.0
B-IV-2	4.55		-3.3		-3.3

5. Conclusion

Analysis of theoretical and experimental data suggests that the proposed mathematical model and method of calculating the load-bearing capacity of reinforced concrete structures reinforced with combined reinforcement, sufficiently takes into account the design features of these structures. Proposed methodologies can be used in design, modeling and evaluation of their load-bearing capacity and deformability, as well as in the production engineering of reinforced concrete elements. Deviations between experimental data and theoretical results of bearing capacity - 5.9%, crack formation - 7.0%, deformability at 0,7M_{dr2} - 14.3%.

Reference

Azizov, T., Kochkarev, D., Galinska, T., Melnyk, O., 2020. Calculation of Composite Bending Elements. Lecture Notes in Civil Engineering, 181, 25-33. DOI: 10.1007/978-3-030-85043-2_3

Azizov, T., Melnik, O., Myza, O., 2019. Strength and deformation of combined beams with side reinforced plates. Materials Science Forum, 968, 234-239. DOI: 10.4028/www.scientific.net/MSF.968.234

Blikharsky, Y., Selejdak, J., Kopsiika, N., 2021. Corrosion fatigue damages of rebars under loading in time. Materials, 14(12), 3416. DOI: 10.3390/ma14123416.

Blikharsky, Y., Selejdak, J., Kopsiika, N., 2021. Specifics of corrosion processes in thermally strengthened rebar. Case Studies in Construction Materials, 15, e00646. DOI: 10.1016/j.cscm.2021.e00646.

Blikharsky, Y., Selejdak, J., Kopsiika, N., Vashkevych, R., 2021. Study of Concrete under Combined Action of Aggressive Environment and Long-Term Loading. Materials, 14(21), 6612. DOI: 10.3390/ma14216612.

Blikharsky, Y., Vashkevych, R., Kopsiika, N., Bobalo, T., Blikharsky, Z., 2021. Calculation residual strength of reinforced concrete beams with damages, which occurred during loading. In IOP Conference Series: Materials Science and Engineering 1021 (1), 012012. DOI: 10.1088/1757-899X/1021/1/012012.

Blikharsky, Z., 2019. Research into glue materials for repairing the cross-section of RC beams. Budownictwo o zoptymalizowanym potencjale energetycznym, 8(2), 63-68. DOI: 10.17512/bozpe.2019.2.07

Blikharsky, Z., Vegera, P., Vashkevych, R., Shnal, T., 2018. Fracture toughness of RC beams on the shear, strengthening by FRCM system. MATEC web of conferences, 183, 02009. DOI: 10.1051/mateconf/201818302009

Borysiuk, O., Ziatiuk, Y., 2020. Experimental Research Results of the Bearing Capacity of the Reinforced Concrete Beams Strengthened in the Compressed and Tensile Zones. Lecture Notes in Civil Engineering, 100, 63-70. DOI: 10.1007/978-3-030-57340-9_8

Czajkowska, A., Raczkiewicz, W., Bacharz, M., Bacharz, K., 2020. Influence of maturing conditions of steel-fibre reinforced concrete on its selected parameters. Budownictwo o zoptymalizowanym potencjale energetycznym, 9(1), 47-54. DOI: 10.17512/bozpe.2020.1.05

Federowicz, K., Techman, M., Sanytsky, M., Sikora, P., 2021. Modification of lightweight aggregate concretes with silica nanoparticles. A review. Materials, 14(15), 4242. DOI: 10.3390/ma14154242

Illytsky, B., Bobalo, T., Kramarchuk, A., 2020. Bearing Capacity of Stone Beam Reinforced by GFRP. Lecture Notes in Civil Engineering, 100, 42. DOI: 10.1007/978-3-030-57340-9_6

Karpiuk, V., Somina, Y., Karpiuk, F., Karpiuk, I., 2021. Peculiar aspects of cracking in prestressed reinforced concrete T-beams. Acta Polytechnica, 61(5), 633-643. DOI: 10.14311/AP.2021.61.0633

Khmil, R.Y., Tytarenko, R.Y., Blikharsky, Y.Z., Vegera, P.I., 2021. Improvement of the method of probability evaluation of the failure-free operation of reinforced concrete beams strengthened under load. IOP Conference Series: Materials Science and Engineering, Vol. 1021(1), 012014. DOI: 10.1088/1757-899X/1021/1/012014

Khmil, R., Tytarenko, R., Blikharsky, Y., Vegera, P., 2020. The Probabilistic Calculation Model of RC Beams, Strengthened by RC Jacket. Lecture Notes in Civil Engineering, 100, 182-191 DOI: 10.1007/978-3-030-57340-9_23

Kos, Z., Klymenko, Y., Karpiuk, I., Grynyova, I., 2022. Bearing Capacity near Support Areas of Continuous Reinforced Concrete Beams and High Grillages. Applied Sciences, 12(2), 685. DOI: 10.3390/app12020685

Koteš, P., Vičan, J., 2021. Influence of Fatigue Crack Formation and Propagation on Reliability of Steel Members. Applied Sciences, 11(23), 11562. DOI: 10.3390/app112311562

Koteš, P., Vavruš, M., Moravčík, M., 2021. Diagnostics and Evaluation of Bridge Structures on Cogwheel Railway. Lecture Notes in Civil Engineering, 200, 93-101. DOI: 10.1007/978-3-030-91877-4_11

Lobodanov, M., Vegera, P., Blikharsky, Z., 2019. Influence analysis of the main types of defects and damages on bearing capacity in reinforced concrete elements and their research methods. Production Engineering Archives, 22, 24-29. DOI: 10.30657/pea.2019.22.05

Maliková L., Miarka P., Šimonová H., Kucharczyková B., 2020. Deflection of an eccentric crack under mixed-mode conditions in an SCB specimen. Construction of Optimized Energy Potential (CoOEP), 9(2), 79-87. DOI: 10.17512/bozpe.2020.2.09

Mao, Y., Shao, C., Shang, P., Li, Q., He, X., Wu, C., 2019. Preparation of high strength PET/PE composites reinforced with continued long glass fibers. Materials Research Express, 6(4), 045303. DOI: 10.1088/2053-1591/aace48

Panchenko, S., Fomin, O., Vatulia, G., Ustenko, O., Lovska, A., 2021. Determining the load on the long-based structure of the platform car with elastic elements in longitudinal beams. Eastern-European Journal of Enterprise Technologies, 1(7), 109. DOI: 10.15587/1729-4061.2021.224638

Pavlikov, A., Pinchuk, N., Kachan, T., 2020. Strength of Masonry Indirectly Reinforced by Expanded Steel Sheets. Lecture Notes in Civil Engineering, 181, 303-311. DOI: 10.1007/978-3-030-85043-2_29

Song, L., Liu, J., Cui, C., Liu, R., Yu, Z., 2022. Multi-factor sensitivity analysis of chloride ingress: A case study for Hangzhou Bay Bridge. Construction and Building Materials, 330, 127089. DOI: 10.1016/j.conbuildmat.2022.127089

Vavruš, M., Bujňák, J., Koteš, P., 2019. Experimental verification of real behavior of bridge structures using proof-load tests. Pollack Periodica, 14(1), 75-84. DOI: 10.1556/606.2019.14.1.8

Vegera, P., Vashkevych, R., Blikharsky, Y., Khmil, R., 2021. Development methodology of determining residual carrying capacity of reinforced concrete beams with damages tensile reinforcement which occurred during loading. Eastern-European Journal of Enterprise Technologies, 4(7), 112. DOI: 10.15587/1729-4061.2021.237954

钢筋混凝土组合梁应力应变状态的数学建模

關鍵詞

组合钢筋
高强度钢筋
钢混结构
RC 结构设计
外部钢筋

摘要

大多数用于建筑结构计算的现代计算机软件都基于数学相关性，这使得分析承受载荷的结构相当复杂的应力-应变状态成为可能。通常，计算基于有限元法，并简化为使用材料的实际应变图、混凝土和钢筋的 $\sigma - \varepsilon$ 图计算由于外力作用而在结构中产生的变形。现代钢筋混凝土结构计算规范也是以变形模型为基础，采用尽可能接近真实的材料变形图。因此，本研究旨在根据 DBN B. 2. 6-98:2009 和 DSTU 的数学方法和规定，更详细地研究钢筋混凝土结构中发生的过程的应力-应变状态和物理本质。B. 在 2. 6-156:2010 中。即，在研究中分析了用于生产钢筋混凝土构件的 S245 钢带和 A1000 钢筋的组合钢筋。将数学建模结果与根据 DBN B. 2. 6-98:2009 和 DSTU B. B. B 2. 6-156:2010 的计算结果以及现场试验数据进行了比较。因此，可以得出结论，是否有可能使用这种技术以足够的精度来计算组合配筋的钢筋混凝土结构。
